A Focus Control System Based on Varifocal Mirror for CO_2 Fiber-Coupled Laser Surgery

Andre Geraldes, Paolo Fiorini, *Life Fellow, IEEE*, and Leonardo S. Mattos, *Senior Member, IEEE*

***Abstract*—Fiber-coupled laser tools combine the precision of lasers with the flexibility of optical fibers. They have been used in surgical procedures, such as transoral microsurgery, to perform precise incisions in delicate structures that are often difficult to reach with other tools. Unfortunately, the performance of fiber tools is not akin to that of traditional laser systems. Prioritizing miniaturization, these tools typically use no optics and ablate tissue in near-contact mode, which induces significant level of tissue carbonization. To avoid this problem, we have developed a focus control system designed for fiber-coupled laser tools based on a microfabricated varifocal mirror. We have demonstrated the efficiency of the system by adjusting the focusing of a CO_2 laser beam when ablating plaster block targets while varying the distance to the target within the range of 10 mm to 25 mm. The proposed system was able to ablate uniform lines, with an average width of 420 μm and showed higher precision than fixed focus and bare fiber systems.**

***Index Terms*—Laser microsurgery, auto-focusing, varifocal mirror, fiber-coupled lasers.**

I. Introduction

LASER tools have been used in surgical procedures for almost four decades now. One of their main advantages is the ability to perform precise incisions with minimum damage to the surrounding tissue, which makes them especially useful in delicate procedures. One example is transoral laser microsurgery, which is the gold standard treatment for vocal cord tumor [1]–[3]. More recently, we have seen the development of fiber-coupled laser tools [4], in which the laser beam is delivered to the target through a flexible optical fiber, instead of an articulated arm with a series of mirrors. This allowed integrating lasers in endoscopic or minimally invasive tools, expanding its applicability to all kinds of surgical procedures.

Unfortunately, these fiber tools do not show the same level of performance of traditional free beam laser systems. Prioritizing miniaturization, fiber tools typically do not include any optics, ablating tissue by placing the fiber tip in close proximity to the target. This near-contact ablation method induces a significant amount of tissue carbonization, which creates scar tissue that not only hinders the recovery of the patient, but may also result in loss of function for speaking or swallowing [5], [6]. Moreover, bringing the fiber close to the tissue incurs in other issues such as: occlusion of the target being ablated, risk of damage to the fiber tip and increased risk of spreading the tumorous tissue in case of contact with the tool.

These problems can be avoided if the tool is kept away from the tissue and the laser beam is focused at the tissue surface. In fact, previous studies [7] have shown that focused ablation results in higher precision and lower tissue carbonization than near-contact ablation. The main challenge for that is to guarantee the precise focusing of the laser [8]. In a fixed focus system, this requires constantly adjusting the position of the fiber tool, which can be difficult to perform reliably and ultimately ends up increasing the mental workload for the surgeon. On the other hand, with a dynamic focusing system, the focal length of the beam could be adjusted independently, allowing more freedom on the maneuvering of the fiber tool. Besides that, the use of an advanced optical system allows the integration of other features to the laser tool such as auto-focusing of the beam and fast laser scanning.

Therefore to achieve high precision, fiber-coupled laser tools must be integrated with optical systems with dynamic focusing capabilities. This is difficult to achieve because of the limited space available in endoscopic laser tools. In fact, focusing systems based on moving lenses or mirrors are not suitable for that, for being too large and bulky and providing limited potential for miniaturization. An alternative solution to that is to make use of adaptive optical components, such as microfabricated membrane-based varifocal mirrors, which have already been used for imaging applications such as confocal microscopy [9].

Membrane-based varifocal mirrors (VM) are thin reflective membranes that can be dynamically deformed, allowing to change the optical power of the mirror and consequently the focal length of the reflected beam without the need for physical displacements. Several actuation mechanisms [9]–[15] have been proposed to control the deformation of these membranes, resulting in VMs with different operating conditions and different levels of optical power range (OPR). In electrostatic VMs, the mirror's deformation is controlled by applying high voltage between the mirror's surface and a counter electrode embedded in the VM. This actuation mechanism is simple and easy to fabricate, since the membrane and the counter electrode can be made in a single wafer, and can reach more than 80 kHz of actuation frequency [10]. Their main drawback is that they provide limited OPR, due to the weak nature of

Manuscript received January 31, 2021; revised October 13, 2021; accepted October 24, 2021. Date of publication October 28, 2021; date of current version November 19, 2021. This article was recommended for publication by Associate Editor E. Vander Poorten and Editor P. Dario upon evaluation of the reviewers' comments. *(Corresponding author: Andre Geraldes.)*

Andre Geraldes and Leonardo S. Mattos are with the Department of Advanced Robotics, Istituto Italiano di Tecnologia, 16163 Genoa, Italy (e-mail: andre.geraldes@iit.it).

Paolo Fiorini is with the Department of Computer Science, University of Verona, 37134 Verona, Italy.

Digital Object Identifier 10.1109/TMRB.2021.3123672

electrostatic force. While small electrostatic VMs (1 mm of diameter) can reach an OPR of 40 m^{-1} [10], mirrors larger than 3 mm achieve less than 10 m^{-1}, even with an actuation voltage of 350 V [9].

Other actuation mechanisms include piezoelectric VMs, which contain bimorph membranes made with piezoelectric material. In this case, the mirror deformation is not controlled by lateral deflection, but by applying different levels of expansion to each layer of the membrane, causing it to bend. These mirrors can operate with less than 30 V [11] and achieve large deflection in resonant mode, but provide very limited static deflection. Therefore they tend to be more appropriate for oscillating systems. Similarly, electrothermal mirrors are made of bimorph membranes made from materials with different coefficients of thermal expansion, and can control their curvature directly by heating up the membrane. These mirrors can achieve large OPR and operate at frequencies higher than 100 Hz [12], as long as the diameter of the mirror remains lower than 1 mm.

Finally, pneumatic and hydraulic VMs control the deflection of the mirror by using fluid to apply a pressure difference to the membrane. The pressure on the fluid can be controlled by embedding linear actuators on the device, using magnetic [13] or electrostatic actuation [14], or by using a microfluidic channel connected to a pump [15]. The main advantage of this method is that the mirror deformation is parabolic, which results in optimal focusing. Also it is possible to achieve large OPR even for mirrors with large diameter. In [14], a 4 mm pneumatic-electrostatic VM achieved an OPR of 21 m^{-1}, while in [15] a 3 mm hydraulic VM achieved more than 50 m^{-1} of OPR .

Despite their potential, the use of VMs with high-power lasers has never been demonstrated. This can be partly explained by the high thermal sensitivity of most membrane-based varifocal mirrors, since irradiation of a high-power laser can affect the deformation of the VM. This is most significant in small VMs, where the energy of the laser must be concentrated in a small area. Here we aim to tackle this challenge with the development of a hydraulic VM, such as presented in [15], since it is able to achieve large OPR even if the mirror's diameter is large.

In this work we developed a focus control system designed for high-power CO_2 lasers based on the microfabricated hydraulic VM presented in [15]. We characterize the presented system by several laser ablation experiments, which represents a significant contribution in respect to the previous version of the system (which was only compatible with visible light). We also propose a sensorless auto-focus controller based on the deflection model of the VM. These two components are key for enabling a compact auto-focusing system.

The rest of the manuscript is organized as follows. Section II presents the design and model of the focus control system. Section III describes the fabrication method of the VM and the focus control tool. Section IV presents the calibration procedure used to identify the parameters of the auto-focusing controller, while Section V presents the laser ablation validation experiments. Section VI analyzes and discusses the experimental results. Finally, Section VII presents final remarks and perspectives of future work.

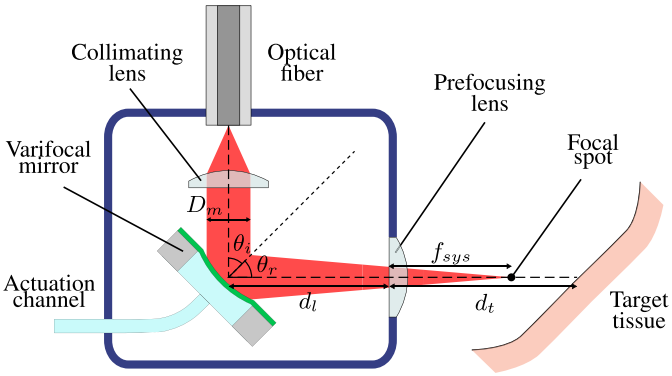

Fig. 1. Schematic diagram of the proposed focus control system based on a microfabricated varifocal mirror.

II. Focus Control System Design

A. Design of the Focus Control System

The design of the proposed focus control system (FC system) is shown in Fig. 1. The laser coming from the optical fiber is collimated by the collimating lens and directed towards the varifocal mirror with an angle of incidence θ_i. The varifocal mirror is used as an off-axis mirror, which means it can focus the laser beam while reflecting it at an angle $\theta_r = \theta_i$. The reflected beam passes through the prefocusing lens and gets focused near the target tissue. In this way, the focal length of the system f_{sys} is given by

$$f_{sys} = \frac{f_l(f_m - d_l)}{f_l + f_m - d_l}, \tag{1}$$

where f_m is the effective focal length of the varifocal mirror, f_l is the focal length of the prefocusing lens and d_l is the distance between the varifocal mirror and the prefocusing lens.

The diameter of the focused laser spot is determined by the numerical aperture of the beam, which is given by

$$NA = \frac{D_m}{2f_l}\left(\frac{f_m + f_l - d_l}{f_m}\right), \tag{2}$$

where D_m is the diameter of the collimated beam. This means that the diameter of the focused laser spot changes with the focal length of the mirror. In order to focus the laser beam at different distances, while keeping the diameter of the focused spot constant, we need the numerical aperture of the beam to be independent of f_m. To achieve that, it suffices to place the prefocusing lens at a distance f_l from the varifocal mirror ($d_l = f_l$), in which case NA becomes $NA = D_m/(2f_l)$. With this constraint, the expression for the focal length of the system reduces to

$$f_{sys} = f_l - P_m f_l^2, \tag{3}$$

with $P_m = 1/f_m$ being the optical power of the varifocal mirror.

In this configuration, the prefocusing lens determines the central focal length of the system, while the varifocal mirror applies a focal shift around such point. As it can be seen, the

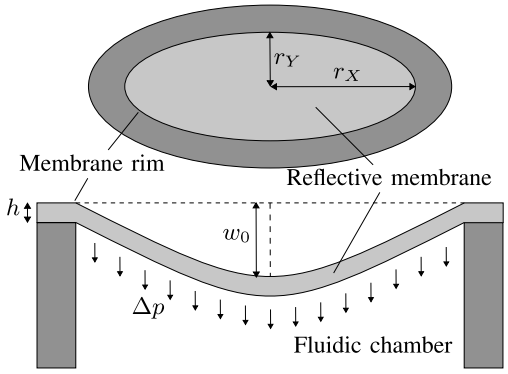

Fig. 2. Schematic representation of an elliptical varifocal mirror deflected by uniform pressure.

applied focal shift to the beam is proportional to the variation in the optical power of the mirror ($\Delta f_{sys} = -f_l^2 \Delta P_m$). This solution is interesting as it greatly simplifies the design of the focus controller. Moreover, it is possible to change the focal range of the system while keeping the same varifocal mirror by simply replacing the prefocusing lens.

B. Focal Length of the Varifocal Mirror

The varifocal mirror used here is an elliptical membrane mirror with hydraulic actuation as shown in Fig. 2. It consists of a free-standing reflective membrane suspended over a fluidic chamber, which can be used to control the pressure applied to the mirror. When uniform pressure Δp is applied to the membrane, the mirror deflects in parabolic shape [16], focusing or defocusing the reflected laser beam, depending on the direction of the deflection (concave or convex). For circular mirrors, the use of an off-axis configuration induces astigmatism on the reflected beam, which degrades the quality of the focusing. However, when the membrane rim is elliptical this effect is compensated [17] as long as we have

$$cos(\theta_i) = \frac{r_X}{r_Y}, \tag{4}$$

with r_X and r_Y being the semi-major and semi-minor axes of the elliptical mirror.

The effective focal length of the varifocal mirror is determined by the central deflection w_0 of the membrane and is given by

$$f_m = \frac{1}{P_m} = \frac{r_X r_Y}{4 w_0}. \tag{5}$$

Finally, the relationship between the pressure difference Δp applied to the membrane and the central deflection w_0 is determined by the resultant elastic stress of the membrane [16] and is given by

$$\Delta p = 2 h r_k w_0 \left(\sigma_0 + \frac{E r_k w_0^2}{3(1-\nu)} \right), \tag{6}$$

where h is the membrane thickness, σ_0 is the residual stress of the membrane, E and ν are the Young's modulus and Poisson's ratio of the membrane material and r_k is given by $r_k = (r_X^2 + r_Y^2)/(r_X^2 r_Y^2)$.

C. Feed-Forward Auto-Focus Controller

The hydraulic actuation system controls the pressure applied to the varifocal mirror by using a microfluidic actuation channel to insert or remove fluid from the fluidic chamber of the mirror. The relationship between the pressure p_a measured in the actuation channel and the pressure difference Δp applied to the mirror's membrane is given by:

$$p_a = p_0 - \Delta p, \tag{7}$$

where p_0 is the hydrostatic pressure determined by the height difference between the fluidic chamber and the measurement point of the actuation channel. The negative sign on the term Δp is given due to the inverse sign notation of the optical power of the mirror (positive optical power indicates a concave mirror, which is obtained by applying a negative actuation pressure in the actuation channel).

With this, the actuation system can control the focal length f_{sys} of the FC system. The goal of the auto-focusing controller (AF controller) is to adjust f_{sys} based on the distance d_t between the target and the FC tool, in order to keep the beam always focused at the target. Therefore the role of the AF controller consists on determining the optimal value of p_a for each value of d_t. By replacing (3), (5) and (6) into (7), we obtain a full model of the FC system as

$$\begin{aligned} p_a(f_{sys}) = {} & f_{sys}^3 \left(K_3 P_l^6 \right) - f_{sys}^2 \left(3 K_3 P_l^5 \right) \\ & + f_{sys} \left(K_1 P_l^2 + 3 K_3 P_l^4 \right) - \left(K_1 P_l + K_3 P_l^3 - p_0 \right) \end{aligned} \tag{8}$$

with $P_l = 1/f_l$ being the optical power of the prefocusing lens and the coefficients K_1 and K_3 being given as

$$K_1 = h \sigma_0 \frac{r_X^2 + r_Y^2}{2 r_X r_Y} \tag{9}$$

and

$$K_3 = \frac{E h \left(r_X^2 + r_Y^2 \right)^2}{96(1-\nu) r_X r_Y}. \tag{10}$$

Since the focusing condition happens with $f_{sys} = d_t$, this allows us to implement a feed-forward controller in which the $p_a(f_{sys})$ curve is used to directly control the FC system. The main advantage of this approach is that it does not require any sensors for measuring f_{sys}. This is important for making the FC system compact, since adaptive optical systems that operate in closed-loop often require the use of beam splitters and optical sensors such as photodetectors or wavefront sensors [18]. However, the drawback of this method is that it is strongly dependent on the accuracy of the model, which may be difficult to guarantee due to the number of parameters involved. To avoid this problem, we used a calibration procedure for identifying the parameters of the AF controller experimentally. This procedure is detailed in Section IV.

III. Fabrication of the Focus Control Tool

A. Fabrication of the Varifocal Mirror

The varifocal mirrors were fabricated in the Clean Room facility of the Italian Institute of Technology (Genoa, Italy),

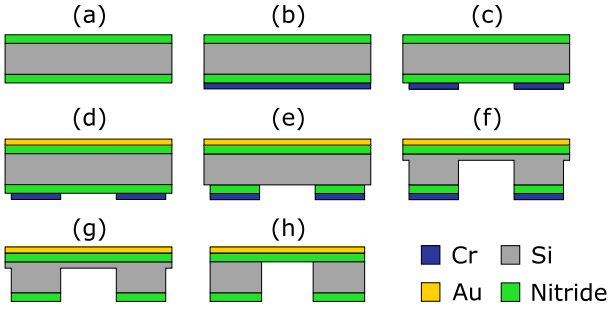

Fig. 3. Schematic diagram of the fabrication process of the elliptical varifocal mirror. (a) Si wafer coated with silicon nitride on both sides. (b) Cr deposition. (c) Cr patterning. (d) Au deposition. (e) Dry etching of the nitride. (f) DRIE of the Si bulk. (g) Cr etching. (h) Si etching with TMAH/IPA solution.

using both bulk and surface micromachining. Fig. 3 shows a schematic diagram of the entire fabrication process. The process starts with a (100) silicon wafer coated with 500 nm of silicon nitride on both sides. The top nitride layer is used as the membrane mirror, while the bottom one is used as a mask for the last etching of the process. To obtain a sealed fluidic chamber beneath the membrane, it is necessary to etch the entire thickness of the wafer from the bottom side. To achieve that, we begin by depositing a 250 nm layer of chromium on the bottom nitride layer. Using photolithography, the chromium layer is patterned with the desired shape for the membrane rim, which in this case is an ellipse with major and minor axes of 4.24 and 3 mm, respectively. This patterning also exposes the edges between adjacent mirrors, to allow dicing the wafer more easily at the end of the fabrication process. After patterning the chromium, we deposit a 200 nm layer of gold on the top nitride membrane to provide high broadband reflectivity to the mirror.

To create the fluidic chamber, we remove the exposed nitride on the bottom layer using dry etching. Then we perform a deep reactive-ion etching (DRIE) to etch the silicon bulk vertically, transferring the pattern of the chromium layer deep into the wafer. To prevent rupturing the top nitride layer, the DRIE is stopped before all the silicon is etched, leaving a remaining silicon layer of approximately 50 µm. This is achieved by measuring the etching rate of the DRIE initially and adjusting the etch duration accordingly. After the DRIE, the chromium mask and the remaining silicon layer are removed using wet etching. The etching of the silicon is performed with a solution of TMAH with 20% of IPA, which allows etching the silicon isotropically. This is important to obtain an elliptical mirror, since anisotropic solutions cause significant distortions to the shape of the membrane rim. Fig 4.a shows a bottom view of a varifocal mirror fabricated with this process.

B. Fabrication of the FC Tool

To control the deflection of the fabricated varifocal mirror, we designed a mirror holder part, as illustrated in Fig. 4.b. The holder contains a square cavity where the mirror can be inserted and a top lid to secure the mirror in place. At the center of the cavity there is a 2 mm microfluidic channel that allows connecting the fluidic chamber of the mirror to the

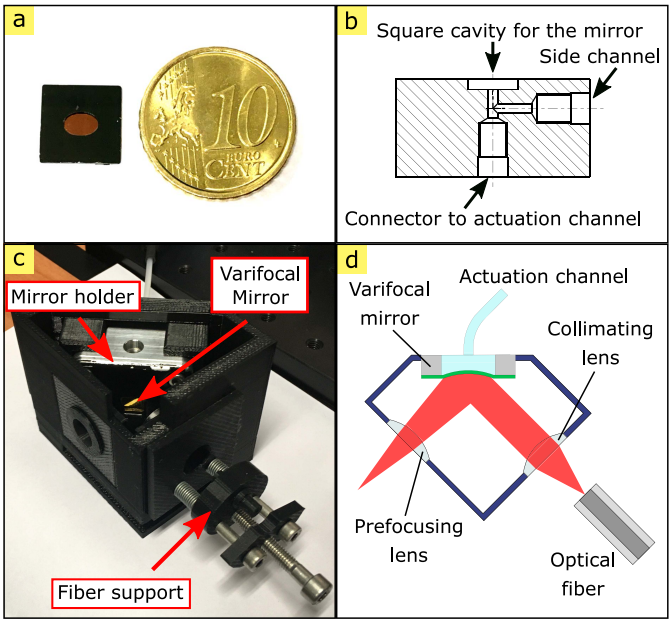

Fig. 4. Fabricated FC tool based on the varifocal mirror. (a) Picture of the fabricated mirror. (b) Schematic diagram of the mirror holder. (c) Picture of the FC tool. (d) Schematic diagram of the FC tool showing the position of the lenses.

actuation channel of the hydraulic system. Once the mirror is inserted, the fluidic chamber can be filled. While doing that, the side channel can be used to extract the air of the hydraulic circuit.

Fig. 4.c shows a picture of the complete FC tool, including the varifocal mirror and the collimating and the prefocusing lenses, while Fig. 4.d shows a schematic representation of the tool, where the position of the lenses can be seen. The mirror holder has been aligned at 45° in respect to each of the lenses, with the major axis of the mirror lying in the plane defined by their optical axes. The collimating and prefocusing lenses were plano-convex ZnSe lenses (which have low absorption for the CO_2 laser beam) with focal lengths of 20 and 15 mm, respectively. The tool has been designed to keep the distance between the prefocusing lens and the axis of the mirror equal to 15 mm, to ensure $d_l = f_l$. Finally, the connector for the optical fiber has been attached to a small linear stage. This was used to adjust the distance between the tip of the fiber and the collimating lens, in order to ensure the beam was properly collimated.

IV. Calibration of the Auto-Focusing Controller

A. Experimental Setup

To calibrate the parameters of the AF controller, we used the experimental setup shown in Fig. 5. The FC tool was attached to an optical breadboard and connected to a hollow silica waveguide with core diameter of 750 μm (Polymicro HWCA7501200 - Molex). The waveguide delivered a 3W continuous-wave laser beam generated by the CO_2 laser system (SmartXide^2 ENT - DEKA). The actuation channel of the FC tool was connected to a custom motorized microinjection system (CellTram vario - Eppendorf) and to a differential

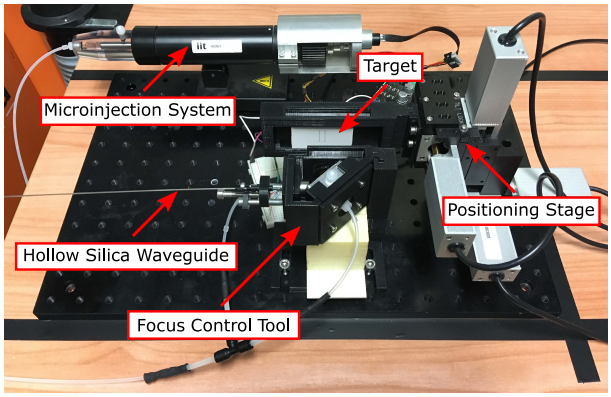

Fig. 5. Experimental setup used for the calibration of the focus control system.

pressure sensor (HSC Series TruStability - Honeywell). The microinjection system and the entire hydraulic circuit have been filled with mineral oil. An Arduino Nano microcontroller, a DC motor driver (MDD10A - Cytron) and a DC motor (GM 20 - Maxon) were used to actuate the microinjection system for controlling the pressure applied to the mirror.

A flat plaster block target was placed in front of the FC tool, perpendicular to the focused laser beam. The target was attached to a linear positioning stage (MX7600 - Siskiyou), which allowed us to move it in the Y (vertically) and Z (propagation of the focused laser beam) directions. Since the positioning stage and the FC tool were fixed, the encoder of the positioning stage was used to calculate the distance d_t between the FC tool and the target, thus simulating an ideal distance sensor. After ablating the plaster block, a Spectral Domain Optical Coherence Tomography (SD-OCT) system (Telesto TEL321C1 - Thorlabs) was used to analyze the quality of the ablation.

B. Experimental Calibration

To determine the AF control curve $p_a(f_{sys})$ that describes the behavior of the developed FC system, we ablated several vertical lines on the target plaster block. The lines were ablated by moving the target in Y and Z simultaneously, such that the distance to target changed linearly along the ablation line. During the ablation, the pressure applied to the mirror was constant, but a different value of actuation pressure was used for each ablation line. Therefore, each line is ablated with different values of p_a and f_{sys}.

Fig. 6 shows a picture of the target after ablating all lines. As it can be seen, the focusing quality of the laser varies along each line. When the distance to the target matches the focal length of the FC system, the ablation width is minimal and the ablation depth is maximal. As the target moves away from that position (in either direction), the ablation width increases and the ablation depth decreases. Therefore, it is possible to measure f_{sys} for each ablation line, by detecting the position of optimal focusing on the line. We performed that by scanning the ablations with the OCT system and analyzing their shapes with a focal point detection algorithm.

For this, each ablation lines was sliced orthogonally to the direction of the line, at every 100 µm. The shape of the ablation

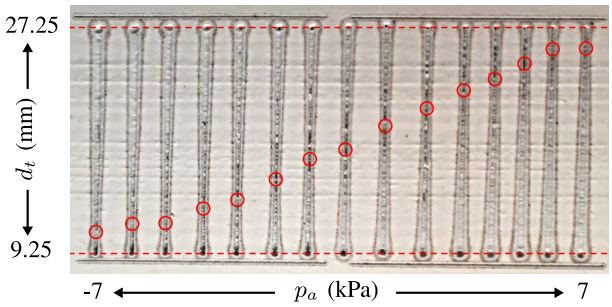

Fig. 6. Vertical lines ablated on a plaster block at variable distance d_t with different values of actuation pressure p_a. The red circles indicate the detected focal position in each line.

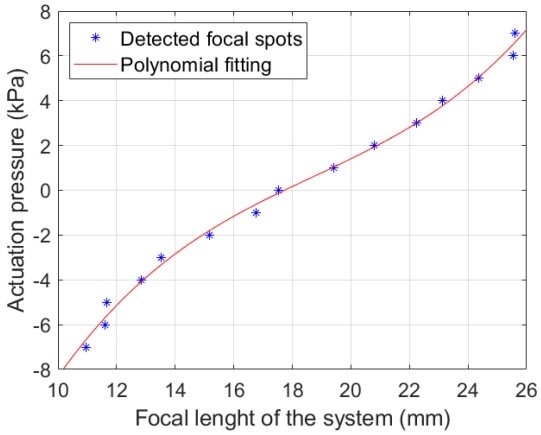

Fig. 7. Actuation pressure of the FC system as a function of the focal length of the system.

in each slice was fitted to a Gaussian curve and the ablation depth and width have been measured as the amplitude of the fitted Gaussian and 6σ, respectively, with σ being the standard deviation of the Gaussian. The depth and width measurements of all segmented slices have been combined into the $depth(x_l)$ and $width(x_l)$ profiles of the line, with x_l being the position along the ablation line. To match these profiles with the range of d_t values used for ablating the targets, we used reference marks at the limits of the lines. At the beginning and end of each line, deep holes were ablated in the plaster, marking the positions corresponding to $d_t = 27.25$ mm and $d_t = 9.25$ mm. Once the $depth(d_t)$ and $width(d_t)$ profiles had been obtained, the focal point f_{sys} for each ablation line has been determined as the d_t value for which the ablation width was minimal.

Fig. 7 shows a plot of all the f_{sys} measurements obtained with this method, with the corresponding actuation pressure used for each ablation line. From these points, we can extract the control curve $p_a(f_{sys})$ of the FC system. Since the relationship between p_a and f_{sys}, defined in (8), is a third degree polynomial, we reduced the model of the FC system to

$$p_a = Af_{sys}^3 + Bf_{sys}^2 + Cf_{sys} + D, \tag{11}$$

with A, B, C and D being coefficients to be experimentally determined. Therefore, by applying a cubic fitting on the obtained measurements of f_{sys} and p_a, we obtain the AF control curve also shown in Fig. 7, with coefficients: $A = 5.44$ Pa/mm^3, $B = -305.51$ Pa/mm^2, $C = 6.33$ kPa/mm

TABLE I
DIRECTION OF MOTION OF THE TARGET IN Y AND Z DURING THE ABLATION FOR EACH ABLATION MODE

Mode	Direction of motion	
	Y	Z
M1	upwards	approaching
M2	upwards	moving away
M3	downwards	approaching
M4	downwards	moving away

and $D = -46.48$ kPa. This curve was used as the feed-forward AF controller for the validation experiments described in Section V.

V. FOCUS CONTROL SYSTEM VALIDATION

To validate the performance of the developed FC system, we conducted three types of experimental analyses. In the first one, we characterized the behavior of the system, to verify that the parameters obtained from the experimental calibration can still be used to control the FC tool even under extended irradiation of the CO_2 laser beam. In the second one, we compared the ablation performance of the tool with and without the AF controller, thus simulating a comparison with an optical tool with fixed focus. In the third analysis, we compared the performance of the FC system to ablations performed in near-contact mode, using only the bare fiber. Sections V-A, V-B and V-C present the details on each of these experiments. After that, Section V-D provides the statistical tests used to verify the significance of the obtained results.

A. Characterization of the obtained Auto-Focusing Controller

To control the FC tool using the proposed feed-forward controller and the experimental parameters obtained in Section IV-B, we must verify that the proposed model is able to accurately describe the FC tool, even after extended irradiation by the CO_2 laser beam. In particular, we are interested in investigating two phenomena, that are not captured in the model. The first one is the presence of hysteresis on the mirror actuation system. The second one is the potential change in the system's properties due to temperature variation in the mirror's surface. The later effect is especially important to inspect, since the damage threshold of the varifocal mirror has not been previously characterized.

To verify if any of these effects occur, the ablations performed in Section V-B were made in four different modes, by alternating the direction of motion in the Y (upwards or downwards) and Z (approaching or moving away from the FC tool) directions. Table I shows the direction of motion of the target during each ablation mode. We later analyzed the difference between the four ablation modes by performing the statistical tests presented in Section V-D. In the presence of hysteresis or variation of the mirror's parameters during the ablation, we expected the ablation modes to provide different ablation results. Conversely, if the difference between the modes is not significant, we can assume both phenomena to be nonexistent or negligible.

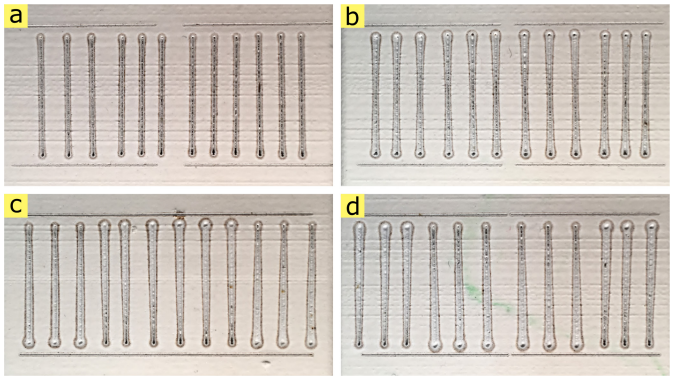

Fig. 8. Plaster block targets ablated with the FC system using (a) the AF controller or fixed focus with p_a equals to (b) 0, (c) 8 kPa or (d) −8 kPa.

B. AF Controller vs Fixed Focus

To compare the AF controller with a fixed focus system, we performed several ablations on plaster block targets in the same manner described in Section IV: by keeping the FC tool fixed and moving the target in Y and Z using the linear positioning stage. In the experiments with the AF controller, the pressure applied to the mirror was changed continuously in order to keep the beam always focused at the target surface. On the other hand, for the fixed focus experiments, constant pressure was applied for the entire ablation line. Three different values of actuation pressure were used, thus configuring three experimental conditions with fixed focus: FF-center ($p_a = 0$), FF-far ($p_a = 8$ kPa) and FF-near ($p_a = -8$ kPa). Ablations were performed in a single pass and the distance between the FC tool and the surface of the target ranged from 9.75 to 25.25 mm. The velocity of the positioning stage in both directions was 1 mm/s. For each experimental condition, we performed 3 ablations with each ablation mode, resulting in a total of 12 ablated lines per condition. Fig. 8 shows pictures of four targets ablated with the AF controller and the fixed focus conditions.

We analysed all ablated targets with the OCT system to extract the depth and width profiles for each ablation line. For each experimental condition, we obtained the average depth and width profiles by calculating the average and standard deviation of the 12 measured profiles. This was done by using linear interpolation on the measured profiles so that the X-coordinates (value of d_t) of all points being averaged were the same. Figs. 9 and 10 show the obtained depth and width profiles for all experimental conditions.

As it can be seen the AF controller was able to achieve more uniform depth and width profiles for the entire distance range. With the AF controller, average ablation depth remained between 590 and 720 µm and average ablation width between 380 and 460 µm. On the other hand, in the fixed focal length cases ablation width increased and depth decreased with the defocusing of the laser. The average depth dropped to 330, 120 and 90 µm and the average width increased to 730, 940 and 890 µm, for the FF-center, FF-far and FF-near cases, respectively. Moreover, the average standard deviation with the AF controller was similar to that of the fixed focus cases. This suggests that this variance is not necessarily caused by

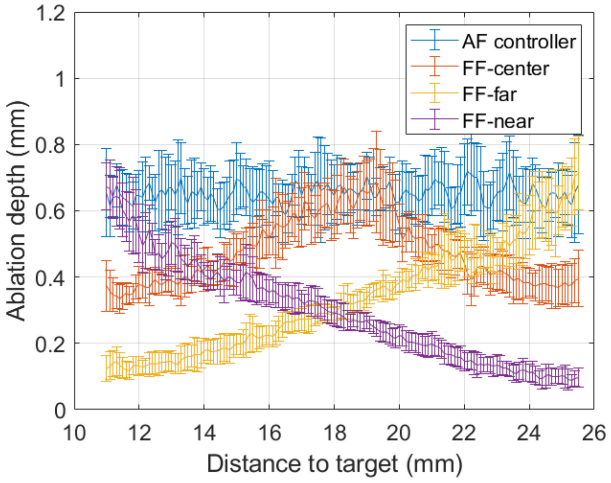

Fig. 9. Depth profiles of the lines ablated on the plaster blocks with and without the AF controller.

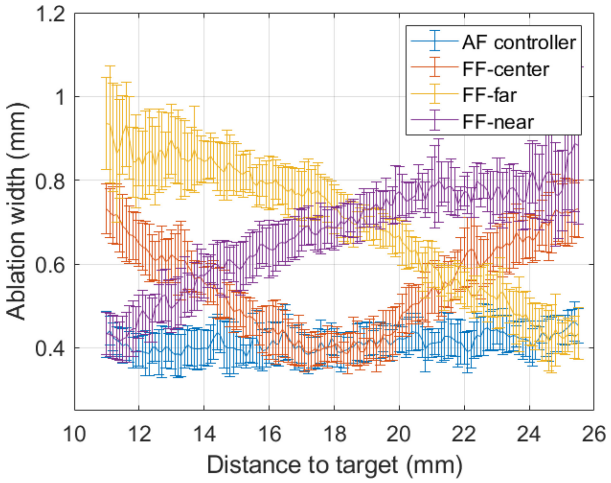

Fig. 10. Width profiles of the lines ablated on the plaster blocks with and without the AF controller.

errors on the model and control of the FC system, but may be associated with other factors such as variation of the output power of the CO_2 laser during the ablation, non-homogeneity of the plaster block along the ablation line and measurement errors when detecting the ablation lines with the OCT system.

C. AF Controller vs Near-Contact Ablation

To compare the performance of our FC system to that of fiber tools without focusing optics, we also performed ablations in near-contact mode. To achieve that, we disconnected the waveguide from our FC system and placed it directly in front of the plaster block target. Then we used the positioning stage to ablate the target vertically, while keeping the distance between the tip of the waveguide and the surface of the target equal to 1 mm. As before, we ablated 12 lines on a plaster block, scanned them with the OCT system and extracted the average depth and width profiles.

Figs. 11 and 12 compare the profiles of the near-contact ablation to those obtained with the AF controller. As it can be seen, the near-contact ablation resulted in lower ablation

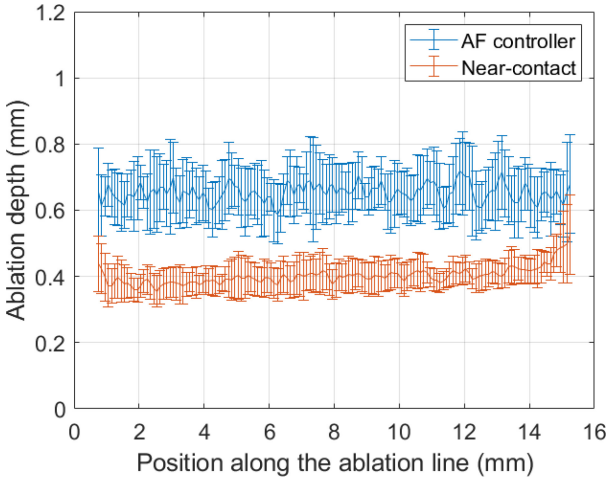

Fig. 11. Depth profiles of the lines ablated on the plaster blocks with the AF controller and in near-contact mode.

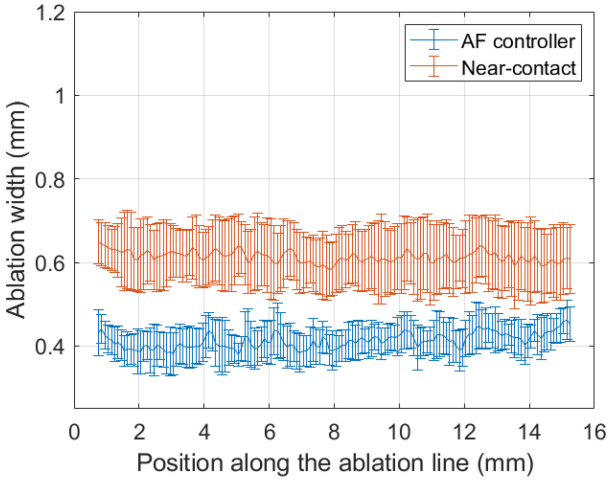

Fig. 12. Width profiles of the lines ablated on the plaster blocks with the AF controller and in near-contact mode.

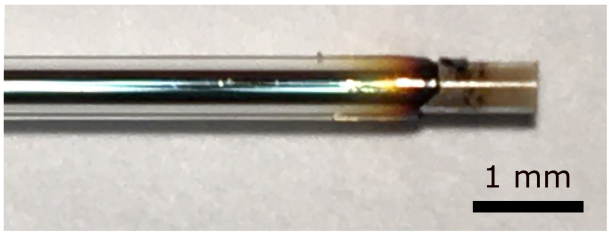

Fig. 13. Tip of the waveguide damaged after the near-contact ablation.

depth (average between 350 and 520 µm) and higher ablation width (average between 580 and 650 µm). Moreover, the ablations in near-contact mode resulted in damage to the tip of the waveguide. Due to the close proximity to the target, the tip of the waveguide overheated, causing its outer acrylate layer to melt and its silica layer to crack. Fig. 13 shows a picture of the waveguide tip after the near-contact ablation experiments.

D. Statistical Significance of the Results

To analyze the statistical significance of the difference between the experimental conditions, while taking into account

TABLE II
STATISTICAL SIGNIFICANCE OF THE ABLATION MODE AND THE DISTANCE TO TARGET ON THE DEPTH AND WIDTH PROFILES OF THE ABLATED LINES

Condition	p-Values of factors	
	Mode	d_t
AF controller	0.8083	0.3538
FF-center	0.1320	1.74×10^{-7}
FF-far	0.0447	7.59×10^{-17}
FF-near	0.4691	4.44×10^{-22}
Near-contact	N/A	0.0044*

TABLE III
STATISTICAL SIGNIFICANCE OF THE EXPERIMENTAL CONDITION ON THE DEPTH AND WIDTH PROFILES OF THE ABLATED LINES

Comparison	p-Value
AF controller vs FF-center	7.72×10^{-12}
AF controller vs FF-far	2.00×10^{-15}
AF controller vs FF-near	3.14×10^{-18}
AF controller vs Near-contact	8.08×10^{-10}
All 5 conditions	2.52×10^{-27}

the variance of all curves, we performed mixed-model analysis of variance (ANOVA) tests [19]. In such test, each ablation line is considered as a single subject with two sets of repeated measures: depth and width. These repeated measures are organized based on two within-subjects factors: the distance to the target (d_t) and the type of measurement (depth or width). Additionally subjects can be divided in groups by between-subjects factors such as the ablation mode or the experimental condition. To limit calculation errors caused by ill-conditioned matrices, the number of levels of the d_t factor has been reduced to 30. This has been done by sampling 30 points of each curve equally spaced in the X direction.

With that method, we performed a 3-way ANOVA test for each of our five experimental conditions. Each test had one between-subjects factor (the ablation mode) and the two within-subjects factors mentioned above. Table II shows the p-values obtained for the ablation mode and the d_t factors. All p-values shown have been adjusted with the Greenhouse–Geisser correction, since the sphericity assumption of the data was not met. For all tests, the normality of the data has been verified by the Shapiro-Wilk test ($p > 0.01$). All calculations have been made using the functions `anova` and `ranova` from MATLAB's Statistics and Machine Learning Toolbox.

As it can be seen, the effect of the ablation mode factor on the outcome of the ablation was not statistically significant ($p > 0.05$) for the cases AF controller, FF-center and FF-near and was barely significant for the case FF-far. This allows us to discard the hypothesis of hysteresis being present on the system. It also allows us to state that the properties of the FC system did not change during the ablation, which indicates that the mirror was not significantly affected by the CO_2 laser irradiation. For the near-contact case, the ablation mode factor does not apply since all ablations were performed in the same way.

Table II also shows the p-values for the d_t factor for each experimental condition. As it can be seen, the distance to the target had a significant impact on the ablation depth and width for all cases except the AF controller. This shows the efficiency of the AF controller, since the variance in the obtained depth and width are not related to the distance to the target. In the case of the near-contact ablation, the p-value shown has been calculated as a function of the position along the ablation line x_l, instead of d_t. For this case, the position along the line had a significant impact on the ablation. This may be associated with the overheating that happened at the tip of the waveguide, which would degrade the quality of the ablation as the waveguide heats up.

We also performed 3-way ANOVA tests to analyze the significance of the experimental condition. These tests were done with one between-subjects factor (the experimental condition) and the same two within-subjects factors, which means the ablation mode factor was ignored (all 12 lines of the same condition were placed in the same group). We performed pair-wise tests between the AF controller and all other conditions and also a complete test with all conditions. Table III shows the p-values obtained for the experimental condition for each test. As before, p-values have been adjusted with the Greenhouse–Geisser correction and normality of data been verified by the Shapiro-Wilk test ($p > 0.01$). As it can be seen, the experimental condition had a significant impact on the ablation depth and width for all tests, even when comparing the AF controller with the near-contact ablation.

VI. DISCUSSION

A. Performance of the FC System

Based on the validation experiments, we can evaluate the performance of the proposed FC system. The main performance metric used here is the uniformity of the obtained focused spot diameter, since this variable is critical to determine the area affected by the laser, as well as the tissue removal rate. Assuming that the diameter of the focused laser spot w was proportional to the obtained ablation width, we can see that the AF controller was able to limit the variation of the spot diameter to 10 % around its central value. On the other hand, in the fixed focus cases, this variation reached more than 120 %. This has two major implications. The first one is the decrease in the precision of the incision, which increases the amount of healthy tissue that must be ablated. The second one is the decrease in the power density of the focused spot, which can change the laser-tissue interaction regime from ablation to coagulation, if the power density becomes too low [20]. In this situation, the surgeon may need to increase the power of the laser, which creates the risk of ablating deeper than expect in certain parts of the ablation line.

When ablating in near-contact mode, the variation of the spot diameter was also low, but the average value of w was 46 % higher than that obtained with the AF controller. This happened because in the near-contact ablation, w is determined by the core diameter of the optical waveguide (which in this case was 750 µm), while with the FC system, it is determined by the numerical aperture of the focused laser

beam, which is given by (2). This means that it is possible to reduce the focal spot diameter by increasing the focal length of the collimating lens (which increases D_m) or decreasing that of the prefocusing lens. The only constraint that must be observed is that the diameter of the collimated beam does not exceed the aperture of the varifocal mirror ($D_m < 2r_Y$). In the system presented here, we measured the value of D_m as approximately 1.5 mm, which means w could still be reduced to half of its size, without changing the prefocusing lens.

In addition to the increased precision, the FC system presents other advantages when compared to the bare fiber. The first one is that keeping a distance between the FC system and the target avoids the thermal damage to the waveguide that was observed in Section V-C. This becomes even more relevant for biological tissue, since chunks of tissue are often ejected during the ablation, which can lead to damage of the fiber tip in case of close proximity. Moreover using a larger distance to the target is also useful when fast scanning systems [21], [22] are integrated in the tool. Since they provide limited angular displacement, these system often require several mm of distance between the target and the tool to provide a significant scanning length. With the FC system, this becomes possible as its central focal length can be adjusted based on the conditions of the clinical application.

Finally, it is important to mention the low sensitivity of the proposed FC system to thermal effects caused by the CO_2 laser. One of the biggest challenges of integrating adaptive optical elements with high-power laser systems are the thermal effects that the laser may cause on the optics. Due to the high power of the laser, even low coefficients of absorption can lead to significant temperature variation, which interfere with the curvature of the optics and can cause complicated effects such as thermal lensing. This is the main reason, why liquid lenses are not suitable for such application, even though they are able to provide a much more compact system than varifocal mirrors. However, in the experiments presented here we did not observe significant change in the deflection model of the mirror during the ablation, since all ablation modes provided equivalent results. This suggests that the temperature of the mirror may change at the beginning of the laser irradiation, but it remains constant during the entire ablation. Moreover, visual inspection of the mirror after the experiments did not indicate any signs of thermal damage to the mirror surface. We attribute such low thermal sensitivity partly to the hydraulic actuation system, since the oil in the fluidic chamber helps dissipating the heat on the membrane of the mirror.

Such low sensitivity to thermal effects provides greater flexibility to the system, allowing it to be used with different tissue removal rates, which can be chosen based on the surgical requirements by modulating the laser power, pulse width, pulse rate, scan speed and laser focus. It is worth mentioning, however, that the damage threshold of the varifocal mirror has not been characterized. Therefore further experimentation will be required in order to determine the maximum power of the laser that can be applied to the system before a drop in the system's performance is observed.

B. Integration With Endoscopic Tool

In order to integrate the proposed FC system in an endoscopic laser tool, two main problems must be addressed: the miniaturization of the tool and the measurement of the distance to the target tissue. Although the FC tool presented here is large, we believe the proposed FC system has great potential for miniaturization. Since the diameter of the collimated laser beam was lower than 2 mm, the dimensions of the varifocal mirror can be reduced even further and the lenses can be replaced by custom lenses of less than 3 mm of aperture. Additionally the mirror holder and all mechanical parts can be significantly miniaturized. The main constraint on the size of the FC tool is the requirement of $f_l = d_l$, which can pose a problem when f_l is relatively large. This however can be compensated by adding a static flat mirror between the varifocal mirror and the prefocusing lens, in such way that the focused beam exits through the front of the tool, parallel to the optical fiber. This way, we believe it is possible to reduce the diameter of the entire tool to less than 10 mm, allowing it to be used in applications such as transoral surgery.

To measure the distance between the target and the tool, we could integrate our FC system with a laser-based distance sensor such as the one proposed in [23], which was developed for fetoscopic laser surgery. This however would increase the size of the tool, since it would be necessary to use a beam splitter for separating the measurement laser from the ablation laser. Another way of measuring the distance to target is to use computer vision algorithms to reconstruct the surface of the tissue using the stereo cameras already present in the endoscopic tool. This has been implemented in [24], where the authors developed a real-time algorithm that was able to reconstruct the surface of the vocal cords and estimate the distance to the target with a precision of 94 µm. The same approach has been used in [25], where preliminary experiments have demonstrated the integration of the FC system presented here with a stereo endoscope. We believe this solution is more suitable for our FC system, since it allows measuring the distance to the target without adding any sensors to our system.

VII. Conclusion

In this paper, we presented a focus control system based on a microfabricated varifocal mirror with hydraulic actuation and validated its performance with a 3W CO_2 laser beam. The developed system was able to successfully adjust the focus of the laser while ablating plaster block targets at a distance range between 9.75 and 25.25 mm. The ablated lines had an average ablation width of 420 µm with a maximum variation of less than 10%. This performance was far superior to that of a fixed focus system for which the obtained ablation width reached 940 µm within the same distance range. The proposed system also performed better than a bare fiber system, achieving lower average ablation width and avoiding any thermal damage to the tool.

In future work we expect to integrate the proposed system in an endoscopic laser tool, by miniaturizing the current prototype and integrating the system with a distance sensor based on 3D surface reconstruction. Although the developed prototype

is still large, the proposed focusing system has great potential of miniaturization since it does not require physical displacement of any of its optical components. We also expect to validate the performance of the proposed system when ablating biological tissue and to compare it with that of existing fiber-coupled laser tools.

REFERENCES

[1] V. Oswal, M. Remacle, S. Jovanvic, S. Zeitels, J. Krespi, and C. Hopper, *Principles and Practice of Lasers in Otorhinolaryngology and Head and Neck Surgery*. Amsterdam, The Netherlands: Kugler Publ., 2014.

[2] M. Rubinstein and W. B. Armstrong, "Transoral laser microsurgery for laryngeal cancer: A primer and review of laser dosimetry," *Lasers Med. Sci.*, vol. 26, no. 1, pp. 113–124, 2011.

[3] L. S. Mattos *et al.*, "μRALP and beyond: Micro-technologies and systems for robot-assisted endoscopic laser microsurgery," *Front. Robot. AI*, vol. 8, p. 240, Sep. 2021.

[4] Z. Wang and N. Chocat, "Fiber-optic technologies in laser-based therapeutics: Threads for a cure," *Current Pharm. Biotechnol.*, vol. 11, no. 4, pp. 384–397, 2010.

[5] P. Janda, R. Sroka, B. Mundweil, C. S. Betz, R. Baumgartner, and A. Leunig, "Comparison of thermal tissue effects induced by contact application of fiber guided laser systems," *Lasers Surg. Med.*, vol. 33, no. 2, pp. 93–101, 2003.

[6] L. Presutti, "Deglutition and phonatory function recovery following partial laryngeal surgery: Speech therapy methods and surgical techniques," *Acta Otorhinolaryngologica Italica*, vol. 30, no. 5, p. 235, 2010.

[7] A. Acemoglu and S. L. Mattos, "Non-contact tissue ablations with high-speed laser scanning in endoscopic laser microsurgery," in *Proc. 40th Annu. Int. Conf. IEEE Eng. Med. Biol. Soc. (EMBC)*, 2018, pp. 3660–3663.

[8] D. Kundrat *et al.*, "Toward assistive technologies for focus adjustment in teleoperated robotic non-contact laser surgery," *IEEE Trans. Med. Robot. Bionics*, vol. 1, no. 3, pp. 145–157, Aug. 2019.

[9] S. J. Lukes and D. L. Dickensheets, "Agile scanning using a mems focus control mirror in a commercial confocal microscope," in *Proc. Three-Dimensional Multidimensional Microscopy Image Acquisition Process. XXI*, vol. 8949, 2014, Art. no. 89490W.

[10] R. Hokari and K. Hane, "A varifocal convex micromirror driven by a bending moment," *IEEE J. Sel. Topics Quantum Electron.*, vol. 15, no. 5, pp. 1310–1316, Sep./Oct. 2009.

[11] P. Janin, R. Bauer, P. Griffin, E. Riis, and D. Uttamchandani, "Characterization of a fast piezoelectric varifocal MEMS mirror," in *Proc. Int. Conf. Opt. MEMS Nanophoton. (OMN)*, 2018, pp. 1–5.

[12] D. Burns and V. Bright, "Micro-electro-mechanical focusing mirrors," in *Proc. 11th Annu. Int. Workshop Micro Electro Mech. Syst.*, 1998, pp. 460–465.

[13] M. M. Hossain, W. Bin, and S. H. Kong, "Large-stroke convex micromirror actuated by electromagnetic force for optical power control," *Opt. Exp.*, vol. 23, no. 22, pp. 28358–28368, 2015.

[14] M. J. Moghimi and D. L. Dickensheets, "Electrostatic-pneumatic membrane mirror with positive or negative variable optical power," *J. Microelectromech. Syst.*, vol. 24, no. 3, pp. 716–729, 2015.

[15] A. Geraldes, P. Fiorini, and L. S. Mattos, "An auto-focusing system for endoscopic laser surgery based on a hydraulic MEMS varifocal mirror," in *Proc. 19th Int. Conf. Adv. Robot. (ICAR)*, 2019, pp. 660–665.

[16] W. K. Schomburg, "Membranes," in *Introduction to Microsystem Design*. Heidelberg, Germany: Springer, 2011, pp. 29–52.

[17] P. A. Himmer and D. L. Dickensheets, "Off-axis variable focus and aberration control mirrors," in *Proc. MOEMS Display Imag. Syst.*, vol. 4985, 2003, pp. 296–304.

[18] S. Bonora, J. Pilar, A. Lucianetti, and T. Mocek, "Design of deformable mirrors for high power lasers," *High Power Laser Sci. Eng.*, vol. 4, p. e16, May 2016.

[19] S. Murrar and M. Brauer, "Mixed model analysis of variance," in *The SAGE Encyclopedia of Educational Research, Measurement, and Evaluation*, B. B. Frey, Ed. Thousand Oaks, CA, USA: SAGE Publ., 2018, pp. 1075–1078.

[20] A. Acemoglu, L. Fichera, I. E. Kepiro, D. G. Caldwell, and L. S. Mattos, "Laser incision depth control in robot-assisted soft tissue microsurgery," *J. Med. Robot. Res.*, vol. 2, no. 03, 2017, Art. no. 1740006.

[21] A. Acemoglu, D. Pucci, and L. S. Mattos, "Design and control of a magnetic laser scanner for endoscopic microsurgeries," *IEEE/ASME Trans. Mechatronics*, vol. 24, no. 2, pp. 527–537, Apr. 2019.

[22] O. Ferhanoglu, M. Yildirim, K. Subramanian, and A. Ben-Yakar, "A 5-mm piezo-scanning fiber device for high speed ultrafast laser microsurgery," *Biomed. Opt. Exp.*, vol. 5, no. 7, pp. 2023–2036, Jul. 2014. [Online]. Available: http://www.osapublishing.org/boe/abstract.cfm?URI=boe-5-7-2023

[23] T. Seki, K. Oka, A. Naganawa, H. Yamashita, K. Kim, and T. Chiba, "Laser distance measurement using a newly developed composite-type optical fiberscope for fetoscopic laser surgery," *Opt. Lasers Eng.*, vol. 48, no. 10, pp. 974–977, 2010.

[24] A. Schoob, D. Kundrat, L. Kleingrothe, L. A. Kahrs, N. Andreff, and T. Ortmaier, "Tissue surface information for intraoperative incision planning and focus adjustment in laser surgery," *Int. J. Comput. Assist. Radiol. Surgery*, vol. 10, no. 2, pp. 171–181, 2015.

[25] A. Geraldes, V. Penza, and L. S. Mattos, "Towards a compact vision-based auto-focusing system for endoscopic laser surgery," in *Proc. IEEE/RSJ Int. Conf. Intell. Robots Syst. (IROS)*, 2021, pp. 9438–9443.

Andre Geraldes received the B.Sc. degree in mechatronics engineering and the M.Sc. degree in automation and electronic systems engineering from the University of Brasília, Brazil, in 2012 and 2014, respectively, and the Ph.D. degree in computer science from the University of Verona, Italy, in 2019. He is currently a Postdoctoral Researcher with the Biomedical Robotics Laboratory, Istituto Italiano di Tecnologia, Genoa, Italy. His research interests are in the field of medical robotics, including smart medical devices for minimally invasive procedures, laser microsurgery and integration between MEMS devices and surgical robots.

Paolo Fiorini (Life Fellow, IEEE) received the Laurea degree in electronic engineering from the University of Padua, Italy, the M.S.E.E. degree from the University of California at Irvine, USA, and the Ph.D. degree in ME from UCLA, USA. From 1977 to 1985, he worked for companies in Italy and in the USA developing microprocessor-based controllers for domestic appliances, automotive systems, and hydraulic actuators. From 1985 to 2000, he was with NASA Jet Propulsion Laboratory, California Institute of Technology, where he worked on autonomous and teleoperated systems for space experiments and exploration. In 2001, he returned to Italy with the School of Science and Engineering, University of Verona, Italy, where he is currently a Full Professor of Computer Science. In 2001, he founded the ALTAIR Robotics Laboratory to develop innovative robotic systems for space, medicine, and logistics. Research in these areas have been funded by several National and International projects, including the European Framework programs FP6, FP7, H2020, and ERC. His activities have been recognized by many awards, including the NASA Technical Awards.

Leonardo S. Mattos (Senior Member, IEEE) received the B.Sc. degree from the University of São Paulo, São Carlos, Brazil, in 1998, and the M.Sc. and Ph.D. degrees in electrical engineering from the North Carolina State University (NCSU), Raleigh, in 2003 and 2007, respectively. He is a Team Leader with the Istituto Italiano di Tecnologia (IIT), Genoa, Italy. He worked as a Research Assistant with the Center for Robotics and Intelligent Machines, NCSU from 2002 to 2007. He has been a Researcher with IIT's Advanced Robotics Department since 2007. He was the PI and coordinator of the European project RALP and of the project TEEP-SLA. He is currently the PI of the translational project Robotic Microsurgery, which is dedicated to the creation of new technologies for the detection and treatment of diseases in delicate organs. His research interests include robotic surgery, smart medical devices, laser microsurgery, user interfaces, computer vision, and automation.